

# On the inner-shelf circulation in the northern Gulf of Cádiz, southern Portuguese shelf

R.F. Sánchez<sup>a,\*</sup>, E. Mason<sup>b</sup>, P. Relvas<sup>c</sup>, A.J. da Silva<sup>d</sup>, Á. Peliz<sup>e</sup>

<sup>a</sup>CIACOMAR/CIMA, Univ. Algarve, Avda. 16 de Junho s/n, 8700-311 Olhão, Portugal

<sup>b</sup>IPIMAR, A. Brasília, 1449-006 Lisboa, Portugal

<sup>c</sup>FCMA/CIMA, Univ. Algarve, Campus de Gambelas s/n, 8000 Faro, Portugal

<sup>d</sup>Instituto Hidrográfico, Rua das Trinas 49, 1249-093 Lisboa, Portugal

<sup>e</sup>D. Física, Univ. Aveiro, Campus de Santiago, 3810-193 Aveiro, Portugal

Received 1 February 2005; accepted 8 April 2006

Available online 17 August 2006

## Abstract

A new look at the inner-shelf circulation in the northern Gulf of Cádiz (SW Iberian Peninsula) is taken. Results reveal the introduction of a sharp spatial heterogeneity in the wind field by the coastal geometry around Cape St. Vincent and nearby mountain chains. Direct observations taken in November–December 2001 reveal the alternating nature of the coastal flow along the SW Iberian Peninsula, featuring a sharp current inversion on time scales of less than 2 days. Along-shore gradients of the oceanic wind stress were detected, which may contribute to the coastal circulation patterns in the region. Over the observational period, the sea-level variability in the Gulf of Cádiz is better explained by the action of along-shore winds outside the Gulf, than by local winds. This is confirmed by a scale analysis done on the vertically integrated momentum equation. It is shown that, to a first approximation, the expected behaviour of the inner-shelf flow responds to linear dynamics. In this approximation, the along-shore sea-level slope (~5 cm over 100 km) is the dominant term, overriding the linear (bottom and surface) stress terms. This suggests control by large-scale atmospheric pressure systems, and negligible dynamical influence from local wind stress.

© 2006 Elsevier Ltd. All rights reserved.

*Keywords:* Inshore counter-currents; Momentum balance; Shelf circulation; Winter circulation; Continental shelf processes

## 1. Introduction

Located at the northernmost tip of the Eastern Boundary Current System (EBCS) of Western Europe and North Africa, the SW Iberian Peninsula (IP) is noted for the marked geographical anomaly

constituted by Cape St. Vincent. At this point, the western Iberian coast meets, almost at right angles, the southern Iberian coast (Fig. 1), with the additional presence of mountainous peaks of ~900 m relatively close to the coast. A major difference with respect to other well-studied EBCSs, such as the US west coast, is the coastal discontinuity imposed by the Strait of Gibraltar. Through this strait, exchange between the Atlantic Ocean, at the surface, and the Mediterranean Sea, at the bottom, occurs. A key result of this exchange is the

\*Corresponding author. Present address: Instituto Español de Oceanografía (IEO) Promontorio de S. Martín s/n, P.O. Box 240 E-39080, Santander, Spain. Fax: +34 942275072.

E-mail address: rleal@st.ieo.es (R.F. Sánchez).

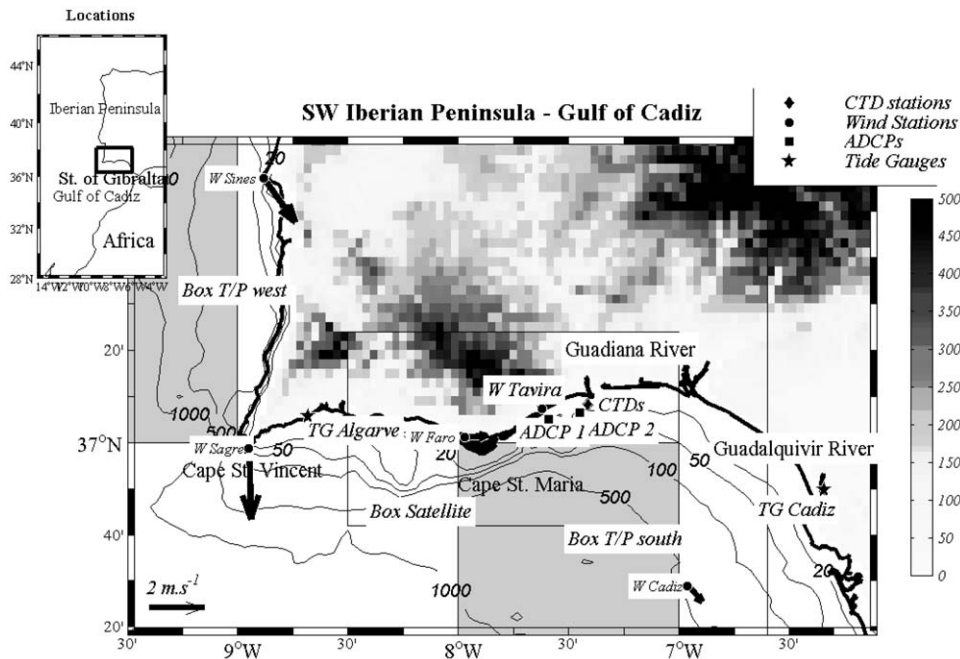


Fig. 1. Map of the Gulf of Cádiz showing topography and locations of the sampling stations. Mean wind vectors over 1999–2001 at the anemometer wind stations are also plotted. The shaded boxes for the satellite images and the T/P altimeter data spatial averages are also shown and indicated. A general location map with geographical details is plotted in the inset.

dissimilar mass field characteristics of the IP system when compared with others. This latter fact has attracted numerous observational programs since the 1950s, and substantial knowledge of the dynamics of the subsurface Mediterranean outflow has been attained. Yet, detailed knowledge of the particularities of the surface circulation of the Gulf of Cádiz remains still poor.

An understanding of the surface ocean circulation in such orographically complex regions requires the determination of the structure of coastal wind fields. These may have a variable spatial structure, influenced either by pure physical interaction with geographic features (sheltering or channelling) or by local-scale modification of the lower-atmosphere stratification at the sea-surface boundary. In the case of the Gulf of Cádiz, the land geometry has been shown to have a rectifying effect on the prevailing wind patterns, with shadowing of the preferential NE–SW wind pattern lee of the Cape, or funnelling and channelling for other patterns (Lobo et al., 2004).

The local-scale oceanographic context of the SW IP has been explored with single-point coastal meteorological wind station data and SST satellite images by Folkard et al. (1997), after Fiúza (1983).

In general, the Gulf of Cádiz has been described as a large bight that is subject to marked recirculations (Sánchez and Relvas, 2003a,b). Conspicuous seasonal alternation of flow and hydrographic fields, with clear upwelling and downwelling seasons over the shelf and the coastal ocean, has been reported. The aforementioned studies observed correlation between the SST and local winds, specially during the summer months when the thermal contrast associated with the coastal upwelling is most evident. The proposed mechanism has been related with air–sea interactions through momentum exchange in the classical Ekman circulation (Fiúza, 1983). Hence, as observed in other EBCSSs, north-erlies (westerlies for the south coast) would favour upwelling, whereas the onset of southerlies (east-erlies) would contribute to the development of poleward flows (Folkard et al., 1997).

These studies have shown that much of the variability over the inner shelf of the northern Gulf of Cádiz can be explained by flows counteracting those at the outer shelf and slope. Sequences of summer SST satellite images are usually dominated by a zonal current pattern formed by poleward and equatorward advection of warm and cold tongues of water, respectively (e.g., Fiúza, 1983; Folkard

et al., 1997; Relvas and Barton, 2002; Lobo et al., 2004), consisting of a warm inshore counter-current opposing the offshore upwelling circulation in the northern Gulf of Cádiz. Winter images show a similar zonal pattern, yet with colder waters over the shelf, associated with-river runoff (Peliz et al., 2004). The counter-current typically extends westwards over the inner shelf from the inner Gulf of Cádiz. It may eventually turn northwards along the western coast after reaching Cape St. Vincent (Relvas and Barton, 2005; see the sequence in Fig. 13). Relvas and Barton (2002) observed this to be one of the most recurrent mesoscale patterns present in at least 45% of (summer) cloud-free images from 1982–1994. The persistent recurrence of this inner-shelf circulation was seen also in the sedimentary record. Lobo et al. (2004) presented results proving the western deflection of the sedimentary wedge of the Guadiana and Guadalquivir rivers in the inner-middle shelf of the Gulf of Cádiz. These authors attributed these sedimentary patterns to the occurrence of westward inshore flows.

Detailed observations by Folkard et al. (1997) noted the lack of correlation between the SST signature and the local winds in the winter months. This was initially attributed to the lack of thermal contrast in the winter SST images. However, the notion of the northern Gulf of Cádiz as a region sheltered from the main offshore wind patterns opens the question as to what does occur over the shelves where local winds are weak relative to other forcing mechanisms. Recent studies (Relvas and Barton, 2002; Sánchez and Relvas, 2005) make the claim for mechanisms, other than direct wind forcing, to be responsible for the development of SST patterns in the Gulf of Cádiz region. The proposed mechanisms are based either on the relaxation of upwelling-favourable winds (Relvas and Barton, 2002) or on interaction with the offshore eddy field (Peliz et al., 2004). In this paper, we suggest that the existence of dissimilar wind patterns on either side of Cape St. Vincent, resulting from orographic deformation, is a significant contributor to the surface circulation under weak to moderate wind conditions.

During November–December 2001 as part of the observational programs of the Portuguese SIRIA project, two Acoustic Doppler Current Profilers (ADCP) were deployed over the inner shelf of the Gulf of Cádiz. These data revealed the sudden onset of a counter-current, which appeared to be un-

correlated with the local wind field. This observation prompted a detailed study to be made into the dynamics of this event, with emphasis on the forcing mechanisms. Thus, the objectives of the present paper are the following: (i) to evaluate the role of the various terms in the along-shore momentum balance obtained using the data set of in situ thermohaline and velocity observations taken in winter 2001; (ii) to attempt to define the mechanisms responsible for the observed structure of the flow; (iii) to understand the influence that the dissimilar coastline alignment on both sides of Cape St. Vincent exerts on the wind field over sheltered regions in the lee of the Cape; and (iv) to determine its effect on the coastal ocean circulation along the northern Gulf of Cádiz.

## 2. Data

### 2.1. The November–December 2001 observations

Within the frame of the Portuguese SIRIA project two RDI 600 kHz upward-looking ADCPs were deployed at ~20 m depth in the Gulf of Cádiz between 25 November and 7 December 2001 (Fig. 1). The instruments were placed about 4 m above the bottom and configured to acquire data in 0.75-m bins. After recovery of the instruments, the upper 10 bins were found to be affected by a high signal-to-noise ratio. Hence, the effectively sampled water depth ranged from 8 to 15 m. These data were complemented with a set of simultaneous observations that included tide gauge and bottom temperature observations at the (ADCP) mooring sites, plus several CTD casts performed in nearby locations during the deployment period. Additionally, AVHRR satellite imagery from the German Remote Sensing Service (Deutsches Zentrum für Luft- und Raumfahrt, DLR) was obtained from their public access gateway (<http://isis.dlr.de/>).

### 2.2. Anemometer-based wind data

Hourly anemometer wind data for the period 1999–2001 were obtained from the locations indicated in Fig. 1, with the exception of the Tavira station, which was specifically set up for the November–December 2001 survey, and was situated close to the ground at the Tavira barrier island. Sines, Sagres and Faro stations are land-based meteorological stations, managed by the Portuguese Instituto de Meteorologia, Lisbon. Sines station is

located on the west coast, 8 m above ground level and 15 m above mean sea level (msl). Sagres station is located at Cape St. Vincent, 6 m above ground level and 40 m above msl. Faro station is close to the shore on the south coast, 7.5 m above ground level and 8 m above msl. Cádiz station is an ocean buoy maintained by the Spanish Puertos del Estado, moored in the Gulf of Cádiz at 450 m over the shelf break. Anemometer winds were height-adjusted and corrected for roughness to the equivalent 10-m neutral-stability winds using the logarithmic profile law. A simple statistical check rejected any outliers lying  $\pm 2.3$  standard deviations from the sample mean.

In order to eliminate tidal and other sub-inertial oscillations where required, scalar and vector time series were low-pass filtered using a cosine-Lanczos filter with a half-power point at 40 h spanning 140 h. Vector time series were compared by using two distinct vector correlation methods: the Crosby et al. (1993) and Kundu (1976) statistics. The vector correlation coefficient  $\rho^2$ , as defined in Crosby et al. (1993), accounts for the contribution of each of the orthogonal wind components. A perfect correlation of two means that two vector series may differ only in a constant offset in direction, and a multiplicative factor in magnitude. In this case, the covariance structure of both series is therefore identical. This property makes it an excellent tool to study the spatial heterogeneities of the wind field. Additionally, the Kundu (1976) vector correlation coefficient ( $R$ ) produces the correlation between the wind speeds of the two series, and a speed-weighted estimate of the mean angle through which the first field would have to be rotated counterclockwise to match the second field. As we will see, the correlation values from these two methods are complementary.

### 3. Results

#### 3.1. Long-term winds along the study area

The change of coastline orientation at the conspicuous point of Cape St. Vincent was expected to exert non-negligible effects on the spatial continuity of the wind field, over sheltered regions in the lee of the Cape. In similar regions, this discontinuity has been revealed as a major mechanism responsible for the generation of local forcing (Oey et al., 2001). In order to study these effects in relation to the circulation in the Gulf we compared hourly vector time series of winds at the four longer-

term anemometer wind stations presented in Fig. 1, using the two vector correlation coefficients. These provided scalar measures of the agreement between the vector data sets. Vector correlations were computed over 777 days from 1999 to 2001 (~19000 hourly points for each series). Tavira winds were unavailable for this period.

The correlations were applied for the hourly original (unfiltered), and for the time series with tides and other sub-inertial oscillations removed (low-pass filtered). The results are presented in Table 1. Both vector correlation coefficients were significantly augmented for the filtered series. The augments ranged between 25% and 40% for the Crosby and 13% and 23% for the Kundu correlations. These were more dramatic when any of the stations sited inside the Gulf of Cádiz were involved. This illustrates the effect of local-scale fluctuations, such as sea breeze or atmospheric tides, on instantaneous winds in the sheltered regions of the Gulf. Wind stations at the central/eastern Gulf of Cádiz, such as Faro or Cádiz, generally lagged the wind series at the west coast by

Table 1  
Crosby et al. (1993) ( $\rho^2$ ) and Kundu (1976) ( $R$ ) vector correlations obtained between the wind station pairs used in this study

	Unfiltered series			Low-pass filtered series		
	( $\rho^2$ )	T. lag (h)		( $\rho^2$ )	T. lag (h)	
	( $R$ )	T. lag (h)	Ph. lag (°)	$R$	T. lag (h)	Ph. lag (°)
<i>Reference station: Sines</i>						
<b>Sagres</b>	<b>1.11</b>		1	<b>1.48</b>		1
	<b>0.76</b>	1	-16	<b>0.87</b>	1	-16
<b>Faro</b>	0.76		2	1.23		2
	0.58	2	-18	0.71	1	-16
<b>Cádiz</b>	0.75		4	1.17		4
	0.59	4	-5	0.73	4	-5
<i>Reference station: Sagres</i>						
<b>Faro</b>	0.79		1	1.15		0
	0.60	1	-38	0.71	0	-38
<b>Cádiz</b>	0.68		3	1.05		2
	0.56	3	-26	0.70	2	-26
<i>Reference station: Faro</i>						
<b>Cádiz</b>	<b>0.85</b>		3	<b>1.44</b>		2
	<b>0.67</b>	3	-14	<b>0.87</b>	3	-14

The considered period is 777 days from 1999 to 2001. Bold type refers to the vector correlations obtained along each perpendicular coast. The 95% confidence bound is 0.11 for the Crosby et al. (1993) and 0.12 for the Kundu (1976) correlation coefficients, respectively.

2–4 h. This indicates that the most common wind patterns have a significant northerly component.

Vector correlations showed that coastal winds were well-correlated along each perpendicular coast (marked in bold type in Table 1). For instance, on the west coast the Sines and Sagres stations showed  $\rho^2 = 1.48$  and  $R = 0.87$ . Similarly, on the south coast the Faro and Cádiz stations showed  $\rho^2 = 1.44$  and  $R = 0.87$ . Disagreement occurred when stations situated at the opposite coast were compared. The plot in Fig. 2 shows the cross-vector correlations of the wind series as a function of the distance between wind stations. A least-squares fit to a Gaussian function is also shown. Poorer correlations were obtained with increasing distance. The pairs aligned along each of the perpendicular coasts showed the best values, well above  $\rho^2 > 1.40$ . In contrast, the cross-correlation of stations along each of the perpendicular coasts was much poorer, always below  $\rho^2 < 1.25$ . Note also the low correlations between the stations located immediately to either side of Cape St. Vincent (Faro and Sagres stations). In spite of the fact that these stations are the closest to each other (87 km), they have a poor  $\rho^2 = 1.15$ .

### 3.2. The November–December 2001 deployments

#### 3.2.1. Description of the wind forcing

As was revealed for the 1999–2001 wind series presented above, the wind forcing during the

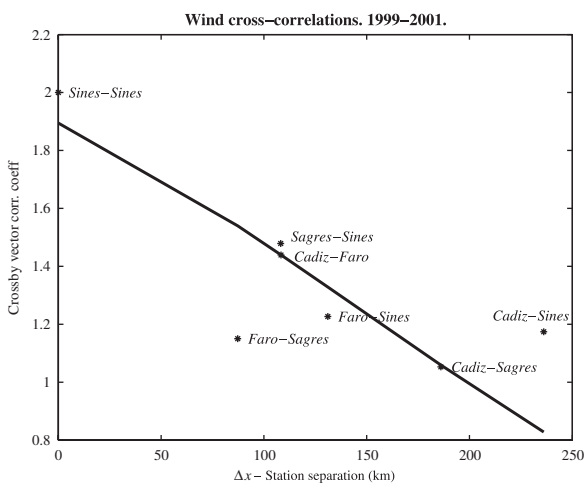


Fig. 2. Crosby et al. (1993) vector cross-correlations between wind stations along the southwestern Iberian Peninsula. The 95% significance bound is less than 0.11 for all cases. A least-squares fit to a Gaussian  $e^{-(\Delta x/D)^2}$  where  $\Delta x$  is the station separation and  $D$  a correlation scale, is also plotted. In this case the correlation scale is 300 km.

deployment period (25 November–7 December 2001) featured dissimilar patterns over both the west and the south coasts. The meteorological stations at Sines and Sagres describe the situation on the west coast (Fig. 3). There, winds were upwelling-favourable from 26 November–1 December, although the northerly component slightly weakened during 29–30 November. After 1 December, until the end of the deployment period, winds showed enhancement of the easterly component with the exception of the interval between 3 and 5 December, when northerlies peaked again. The wind stick diagrams from Faro, Tavira and the Cádiz stations describe the coastal wind conditions inside the Gulf of Cádiz. In contrast to the west coast, winds here were predominantly easterly, hence downwelling-favourable. Exception should be made for two brief periods between 26 and 27 November and 1 and 2 December, when the westerly component prevailed. This situation highlights the disagreement between the coastal winds on either side of Cape St. Vincent. We applied a vector correlation test for this 2-week period. As expected from visual observation, strong disagreement between the vector series north and east of the Cape was found. A very low vector correlation ( $\rho^2 = 0.33$ ) was obtained between Sagres and Cádiz, the Sagres wind leading the Cádiz buoy by 3 h. This value was much smaller than the values observed during the reference 1999–2001 period (Table 1).

To investigate further the spatial continuity of ocean winds during this period we retrieved spatial ocean wind field data to illustrate four significant snapshots of the study period. Fig. 4 presents ocean wind vectors, as obtained from a blend of QuikSCAT swath data and National Centers for Environmental Prediction (NCEP) reanalysis (Chin et al., 1998) derived winds, together with the vectors from the anemometer stations. The QuikSCAT/NCEP data were retrieved from <http://dss.ucar.edu/datasets/ds744.4>. These pictures revealed that over the study period, along the west coast the wind was predominantly blowing from the north, yet with variable intensity, with the exception of the brief period corresponding to December 2. In contrast, the ocean winds were more variable both in direction and magnitude in the Gulf of Cádiz. On November 27 (Fig. 4A) the wind pattern showed a large-scale equatorward wind along the study area, featuring positive wind curl in the Gulf of Cádiz. Three days later (November 30) the wind vectors rotated clockwise, and show an homogeneous NE pattern all across

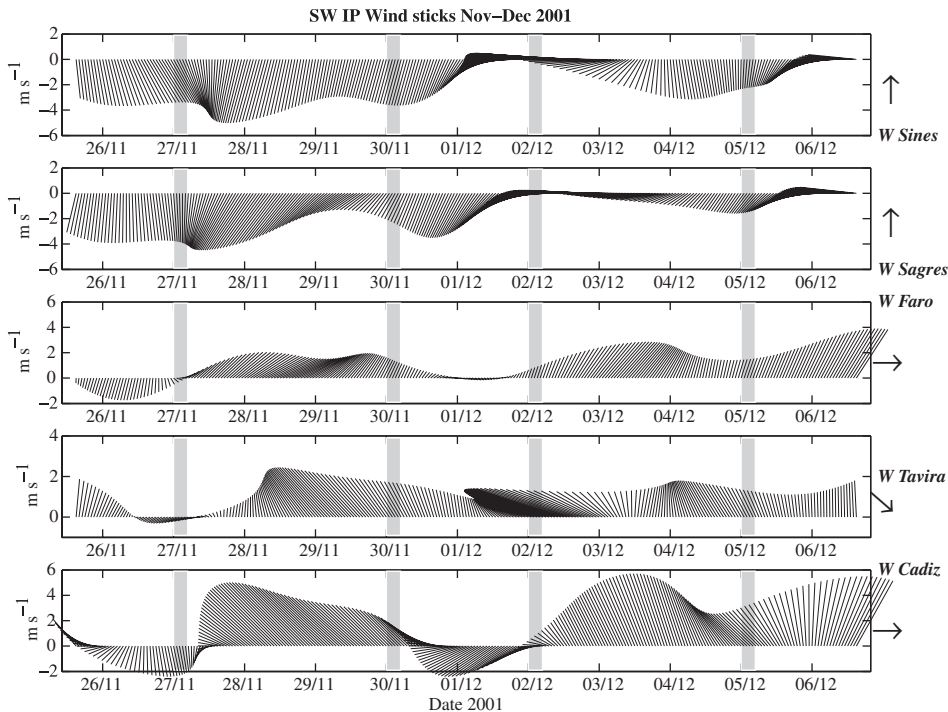


Fig. 3. Wind velocity stick diagrams from the anemometer stations in the Gulf of Cádiz for the November–December 2001 survey. From top to bottom: Sines, Sagres, Faro, Tavira land stations, and Cádiz buoy. Vectors have been conveniently rotated so as to show upwelling-favourable winds as negative. An arrow points to the north in all subplots. All plots have the same scale except for the Tavira winds, which are exaggerated. The area marked in grey is referred to in the text.

the domain. This field illustrates the dissimilar (upwelling-favourable on the west coast and downwelling-favourable on the south coast) wind patterns either side of Cape St. Vincent. On December 2, winds on the west coast rotated to an easterly direction, whilst in the Gulf of Cádiz the winds showed a non-coherent pattern. Finally, on December 5 the wind pattern was similar to the snapshot of November 30, with northerlies along the west coast and easterlies in the Gulf of Cádiz. This field contains evidence of wind shadowing along the northernmost limits of the Gulf of Cádiz and east of Cape St. Vincent.

As shown by the vector correlations and the spatial maps, over the deployment period a clear spatial-temporal break of ocean winds occurred, which appears to be associated with Cape St. Vincent. The wind time series display different behaviour at either side of the Cape, justifying the degradation of the vector correlations between these winds during November–December 2001.

### 3.2.2. Evolution of the temperature field

The temperature time series obtained from the moored instruments together with direct measure-

ments from CTD casts are presented in Fig. 5. In addition, two SST satellite image snapshots corresponding to the deployment period can be seen in Fig. 6. These satellite images reveal that during the described period coastal water was colder than the offshore oceanic water (Fig. 6A). Shelf coastal water in winter usually contains water associated with Guadiana and Guadalquivir runoff (Fig. 7A; e.g. Peliz et al., 2004). Before the deployments (23–24 November) the CTD data showed that the coast east of Cape St. Maria was invaded by waters colder than 16 °C. However, during the deployment period sharp temperature oscillations over small time scales were observed. These were attributed to episodes of advection and retreat of cold water towards and away from the mooring sites. For instance, at the beginning of the sampling period before 27 November, a sharp temperature contrast between the two mooring locations was evident (Fig. 5). The SST image of 26 November (Fig. 6A) permits the inference of a temperature rise at the site of the easternmost instrument, ADCP2, between 23 and 26 November; this indeed occurred as a consequence of the retreat of the coastal water and the

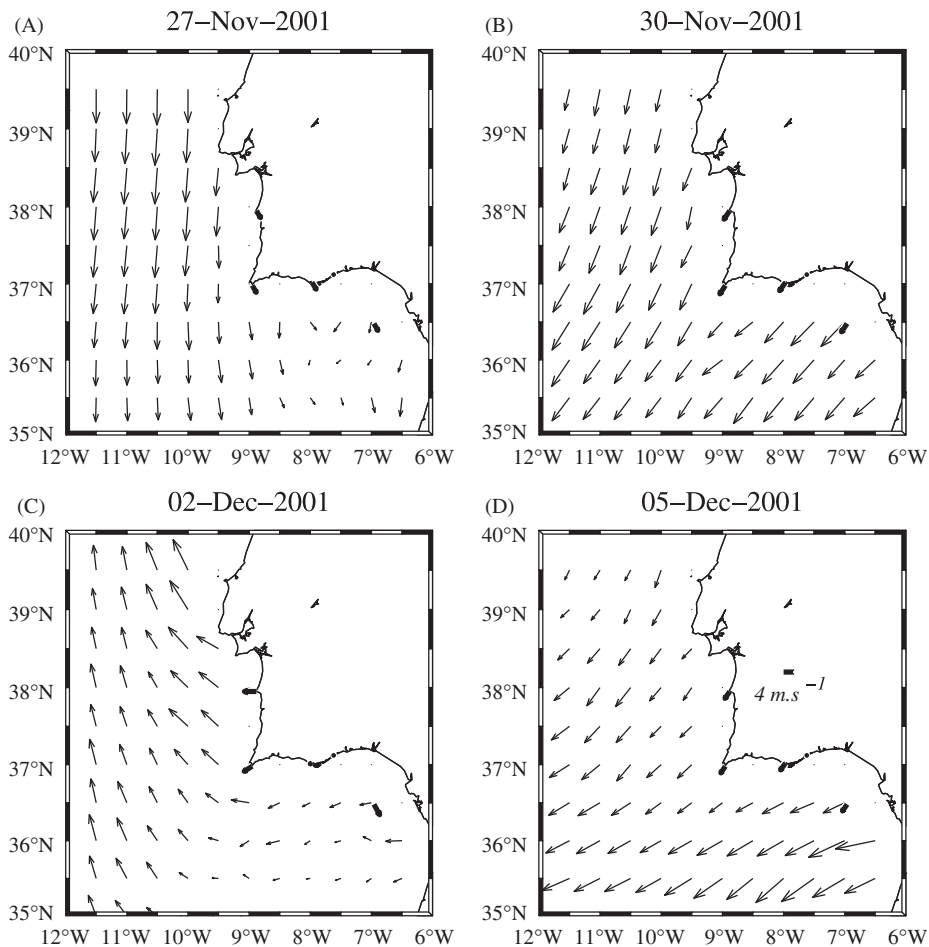


Fig. 4. NCEP/QuikSCAT blend winds for November–December 2001. Wind vectors at the Sines, Sagres, Faro land stations, and the Cádiz buoy anemometer stations are also presented, and correspond to averages over the 24 h prior to the image capture. (A) 27 November; (B) 30 November; (C) 2 December; (D) 5 December. Reference vector is  $4 \text{ m s}^{-1}$ , shown in figure D.

associated onshore and eastward advection of warm, oceanic waters. Hence, ADCP1 (to the west) is situated out of the influence of cold coastal waters, whereas ADCP2 is situated within its influence. The eastward advection of warm water continued during 26–28 November, as shown by the sharp temperature rise detected at ADCP2 (solid line in Fig. 5). This event occurred despite the local mean wind that was blowing from the east (mean values of  $\sim 3 \text{ m s}^{-1}$ ) from 24 to 26 November (see Fig. 6A); instead, it was influenced by equatorward winds of  $\sim 4 \text{ m s}^{-1}$  over the western coast (see Fig. 3).

After this rise, the temperature dropped by  $0.5^\circ\text{C}$  in 2 days (Fig. 5). During this period, strong easterly winds occurred in the Gulf of Cádiz, together with a slight relaxation of northerlies along the west coast

up until 30 November (Fig. 3). This cooling was mostly associated with the westward pushing of cold, coastal waters towards the mooring sites. This temperature fall was disrupted by a slight rise of  $\sim 0.5^\circ\text{C}$  over 24 h between 29 and 30 November, best shown by ADCP1. This latter event occurred during the brief relaxation of easterlies and the westerly wind event in the Gulf of Cádiz.

A dramatic temperature fall of  $1.8^\circ\text{C}$  in less than 36 h was observed at both mooring sites from 30 November to 1 December (Fig. 5). This fall was consistent with the fall observed in CTD casts taken near to the mouth of the Guadiana River at 10 m depth, and the satellite images (Fig. 6B). The satellite image in Fig. 6B was acquired on December 3, but the wind vectors are contemporaneous with the temperature fall, i.e. averaged over 1–2

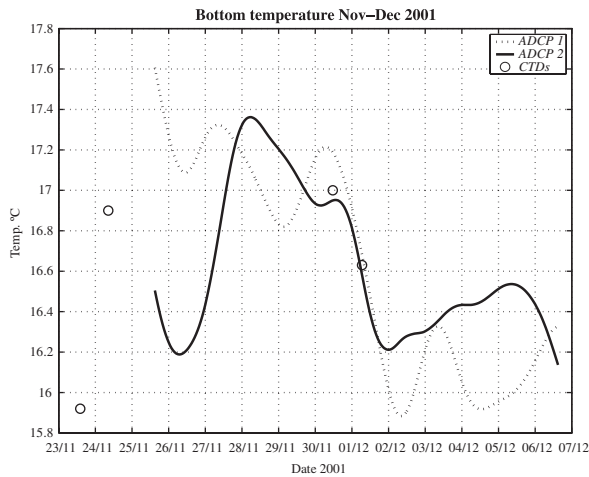


Fig. 5. Bottom temperature time series at the two ADCP mooring sites in November–December 2001. Temperature at the CTD locations is also shown using open circles. The instrument location was about 20 m depth.

December. Westward advection of cold, coastal waters is inferred. Detailed observation of the temperature together with the wind series indicates that this cooling coincided with the relaxation of the local easterlies and the onset of westerlies in the Gulf of Cádiz, and most importantly, with the disruption of the northerlies and the onset of easterlies at the west coast (see Fig. 3).

At the end of the deployment, another temperature rise coincided with a new onset of easterlies, intensified along the Gulf of Cádiz, from 2 December. This event was accompanied by another pulse of northerlies on the west coast. It is most likely that this event occurred as a result of the onshore advance of oceanic water, under the influence of the local easterlies (see Figs. 3 and 4).

This event occurred in the absence of major river discharges (Fig. 7B). To investigate the causes for this event, the temperature time series at the

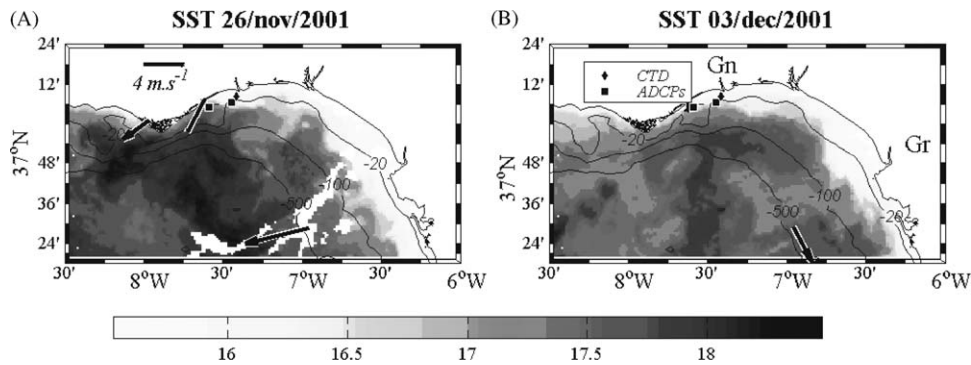


Fig. 6. Daily AVHRR SST composite images and wind vectors in the northern Gulf of Cádiz in 2001. (A) 26 November, (B) 3 December. Locations of the ADCP and CTD stations are also indicated. Wind vectors are averages over the 24 h prior to the image acquisition. Labels Gn and Gr stand for Guadiana and Guadalquivir rivers, respectively. Reference vector is  $4 \text{ m s}^{-1}$ . Colourbar units are  $^{\circ}\text{C}$ .

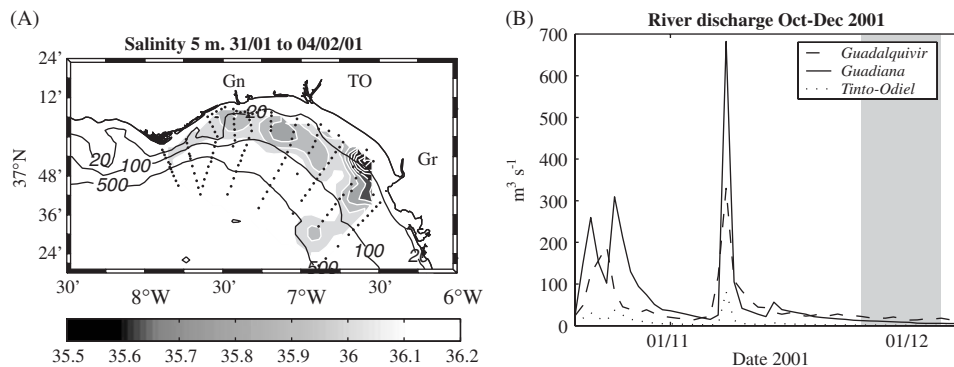


Fig. 7. (A) Surface salinity (depth = 5 m) in the northern Gulf of Cádiz in January 2001. Dots stand for the CTD stations. The 30, 100, 200 and 500 m depth contours are also shown. In this snapshot, the inner shelf appears to be invaded by low salinity waters  $< 36$  of riverine origin. Gn stands for the Guadiana River mouth, TO for the Tinto–Odiel River system and Gr for the Guadalquivir River. (B) River discharges for October–December 2001. The shaded rectangle corresponds to the period 25 November–5 December 2001.

mooring sites was correlated with the wind forcing (Table 2). As can be observed through visual examination of the temperature time series (from any of the sources: ADCP, CTD or satellite), and the winds at various locations in the sampling area, the correlations revealed that shelf water properties in the inner Gulf of Cádiz were poorly correlated with local wind forcing. The temperatures showed better correlation with the wind series at stations situated on the west coast, rather than with local winds in the Gulf of Cádiz. As an example, note that the along-shore wind component at Sines has a correlation of  $-0.84$  with the temperature; the temperature lags behind the wind by about  $\sim 5$  h. The same series compared with the Sagres winds showed a correlation of  $-0.74$ , the wind preceding temperatures by 3–5 h. Conversely, correlations

with local winds at Faro or Tavira showed non-significant values, and weak correlations with the Cádiz winds (0.48 at a lag of +4). These results indicate that large-scale circulation, rather than local winds may be responsible for the thermal patterns found along the inner shelf of the eastern Gulf of Cádiz.

3.2.3. Description of the ADCP velocities

The ADCP observed current patterns obtained from the two instruments were very similar. Examination of the along- and across-shore structure of the currents of ADCP1 showed strong polarisation of the flow, primarily parallel to the isobaths due to the proximity of the coastal wall (Fig. 8A). Mean across-shelf flows were  $< 0.01 \text{ m s}^{-1}$  for all considered bins, which is on the order of magnitude of the accuracy of the ADCP, with standard deviations of  $0.02 \text{ m s}^{-1}$  (Fig. 8B). The along-shore component exhibited more consistent values of  $\sim 0.05 \text{ m s}^{-1}$ . For this reason, velocity vectors were rotated into the direction of maximum variance, and are presented here as the along-shore and across-shore components. Sticks in Fig. 8A represent column-averaged rotated velocity vectors.

Two distinct periods may be distinguished (Fig. 8A). From 26 September to 1 December the current was flowing equatorward (eastward) with maximum subinertial velocities of  $\sim 0.2 \text{ m s}^{-1}$ , although a slight deceleration occurred from 28 to 29 November, accelerating back again on 29–30

Table 2  
Lagged correlations and time lag (hours) between the zonal ( $u$ ) and meridional ( $v$ ) components of the wind and the mean temperature series at the mooring sites for the period 25 November–7 December 2001

	$U$	T. lag (h)	$V$	T. lag (h)
Sines	0.41	0	$-0.84$	$-5$
Sagres	n.s.	n.s.	$-0.74$	$-3$
Faro	n.s.	n.s.	n.s.	n.s.
Tavira	n.s.	n.s.	n.s.	n.s.
Cádiz	n.s.	n.s.	$-0.48$	$+4$

The label 'n.s.' stands for non-statistically significant correlations.

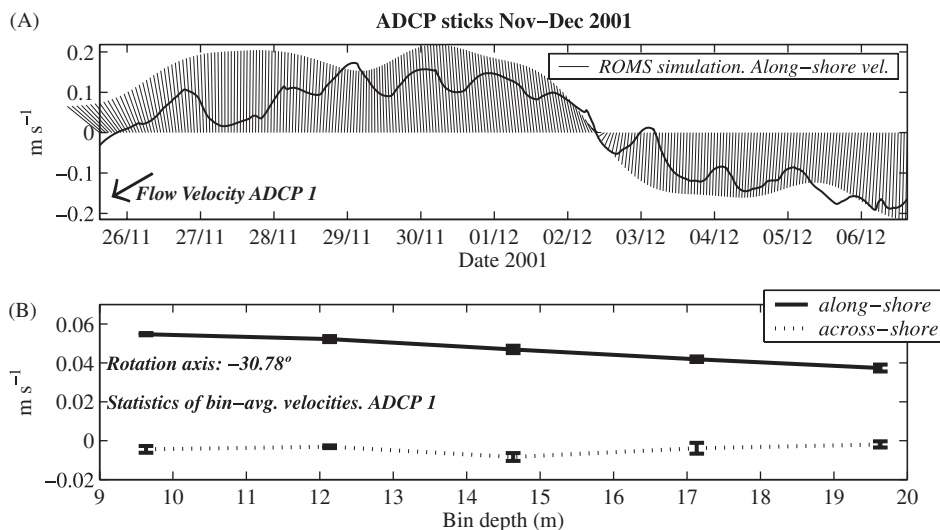


Fig. 8. (A) ADCP1 flow velocity stick plot. Vectors are conveniently rotated into the axis of maximum variance ( $\sim 31^\circ$  anticlockwise). An arrow points to the north for reference. A bold line represents the modelled along-shore velocity at the ADCP1 location. (B) Statistics of the along-shore and across-shore bin averaged velocities. The mean is represented as a line and the standard deviation as an errorbar.

November. The second period occurred from 3 December through to the end of the deployment period; here the current switched to a poleward flow, with velocities at roughly the same order of magnitude as in the previous period. The transition involved a sharp current reversal, from equatorward to poleward flow, that occurred in less than 48 h between 1 and 3 December 2001.

The initiation of the temperature fall described in Section 3.2.2 coincided with the deceleration of the eastward velocities on 28 November, with temperatures remaining low as long as the westward flow continued. This confirms that the dramatic temperature fall was associated with the westward advection of cold water from the eastern Gulf of Cádiz, as also observed in the satellite SST image (Fig. 6). The SST image indicates that this cold water was related to local river runoff. An extreme expression of this feature has been reported by Peliz et al. (2004).

In order to examine the ocean response to the wind stress, we constructed lagged vector correlation of ADCP velocities and wind stress at the different locations. These are presented in Fig. 9. Positive lags stand for the wind leading the ADCP velocities. The Kundu coefficients show a lack of correlation between the ADCP velocities and local winds (Fig. 9A). The best correlations were observed between the ADCP mean vectors and the winds at Sines ( $R = 0.62$ , at  $>20$  h lag), and at Sagres (with  $R = 0.69$ , at 15 h lag) stations, which were located 233 and 123 km, respectively, from the measuring point. In contrast, the nearer Tavira (5 km), Faro (40 km) or Cádiz (80 km) winds, showed lower and non-significant correlations (Fig. 9A). The Crosby coefficient values were generally low. The only significant correlations were obtained for Cádiz winds with a lag of  $\sim 15$  h ( $\rho^2 > 0.8$ ) (Fig. 9B).

The disagreement between the two vector correlation statistics may help us understand the effect of wind on the shelf circulation in the inner Gulf of Cádiz. Each statistic exhibits dissimilar but complementary properties. The method of Kundu (1976) produces complex numbers expressed in terms of  $r_k = R * e^{i*\theta}$ , where  $R$  is the product of the wind speeds between the two fields and  $\theta$  represents a speed-weighted estimate of the mean angle through which the first field would have to be rotated counter-clockwise to match the second field. Hence,  $R$  is a measure of the correlation of the vector magnitudes, and gives a sense of whether the

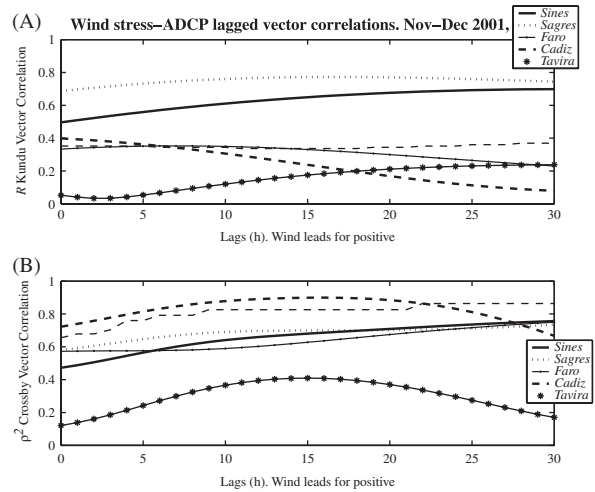


Fig. 9. Lagged ADCP-wind vector correlations for each of the anemometer wind stations along the Gulf of Cádiz during November–December 2001. (A) Kundu (1976) vector correlation coefficient ( $R$ ). (B) Crosby et al. (1993) vector correlation coefficient ( $\rho^2$ ). The 95% confidence bound is indicated as a thin dashed line. The confidence bound in (A) was based on an asymptotic normal distribution of  $0.5 \log((1 + R)/(1 - R) - 1)$ , with an approximate variance equal to  $1/(N - 3)$ ,  $N$  being the number of data points of the series. In (B) the confidence bound was based on the Crosby et al. (1993) results that for a large number of independent samples, the  $\rho^2$  approximates a chi-square distribution with 4 degrees of freedom (dof). The number of independent samples, or effective number of degrees of freedom of the complex series was estimated as in Breaker et al. (1994), based on the e-folding time scale for both orthogonal components, and then choosing the median as a representative time-scale ( $t$ ). After, the dof was estimated as  $dof = N\Delta t \cdot t^{-1}$ ,  $\Delta t$  being the sampling interval (1 h).

differences are more related to speed or direction. The method of Crosby et al. (1993) explores the covariance structure of the orthogonal components of the two vector series, and provides a better overall sense of how well each data series correlates with another over time. This powerful statistic is able to reveal considerable fine structure in the vector correlation sequences, mostly coincident with small changes (Breaker et al., 1994). Thus, the relatively good Crosby correlations of ADCP velocities with (local) winds at Cádiz (Fig. 9B) indicate that small wind oscillations have an effect on the variability of ADCP records locally. Conversely, the low values of the Kundu statistic for the Cádiz winds reflect the fact that there were significant differences in the correlation sequence of ADCP velocities and nearby winds. Instead, the more distant Sines/Sagres winds showed better agreement, in this sense (Fig. 9A). These points

again highlight the underlying effects of phenomena related to the larger-scale wind circulation.

### 3.2.4. The barotropic momentum equation

Local wind-stress variability is insufficient in explaining the observed flow pattern. So what drove the sharp current reversal, and its associated dramatic temperature drop? To determine the mechanisms driving the current reversal, and to account for the observed structure of the along-shore flow field, we considered the vertical integral of the along-shore momentum equation

$$\begin{aligned} & \frac{\partial}{\partial t} \int_{-H}^{\eta'} v \, dz + \frac{\partial}{\partial x} \int_{-H}^{\eta'} uv \, dz \\ & + \frac{\partial}{\partial y} \int_{-H}^{\eta'} v^2 \, dz + f \int_{-H}^{\eta'} u \, dz \\ & = -gH \frac{\partial \eta}{\partial y} - \int_{-H}^{\eta'} \int_z^{\eta'} \frac{g}{\rho_o} \frac{\partial \rho}{\partial y} \, dz' \, dz + \frac{\tau_s^w - \tau_b^b}{\rho_o} \\ & + \int_{-H}^{\eta'} F \, dz. \end{aligned} \quad (1)$$

The coordinate system is with the  $y$ -axis rotated  $31^\circ$  northwards (Fig. 8B) and positive eastward, and the  $x$ -axis directed positive onshore. Hence,  $v, u$  are the along-shore and across-shore components of the velocity,  $\eta$  and  $\eta'$  are the adjusted and actual sea level, respectively,  $\tau_s^w$  and  $\tau_b^b$  are the along-shore components of the surface and bottom stress due to the wind and the bottom friction, respectively,  $F$  is the divergence of the along-shore component of the horizontal Reynold stress,  $H$  is the mean depth (assumed as constant in this case), and  $\rho$  and  $\rho_o$  are the density and mean density, respectively. Assuming barotropic conditions we can integrate and write

$$\begin{aligned} & H \frac{\partial}{\partial t} \bar{v} + H \frac{\partial}{\partial x} \overline{uv} + H \frac{\partial}{\partial y} \bar{v}^2 + Hf\bar{u} \\ & = -gH \frac{\partial \eta}{\partial y} - H^2 \frac{g}{\rho_o} \frac{\partial \rho}{\partial y} + \frac{\tau_s^w - \tau_b^b}{\rho_o} + H\bar{F}, \end{aligned} \quad (2)$$

where the overbar denotes vertical averages.

As in Lentz and Winant (1986) we scaled the terms in the equation of motion (Eq. (2)) using the observations made in the Gulf of Cádiz in November–December 2001. The wind stress  $\tau_s^w$  was parameterised by the quadratic drag law

$$\tau_s^w = \rho_a C_D v_w |\vec{u}_w|, \quad (3)$$

where  $\rho_a$  is air density (assumed to be  $1.22 \text{ kg m}^{-3}$ ),  $\vec{u}_w$  is surface wind velocity vector,  $v_w$  along-shore component of the surface wind velocity ( $\text{m s}^{-1}$ ), and

$C_D$  is a drag coefficient ( $C_D = 0.00114$ , Large and Pond, 1981).

Following Lentz and Winant (1986) and Hickey et al. (2003), the along-shore bottom stress  $\tau_b^b$  was expressed as a linear function of the depth-averaged velocity,  $\bar{v}$ :

$$\tau_b^b = \rho_o r \bar{v}, \quad (4)$$

where  $r$  is a resistance coefficient set to  $r = 1.25 \times 10^{-4} \text{ m s}^{-1}$ .

The along-shore sea-level slope (ASLS) term was estimated using the sea levels from tide-gauges (TGs) located on the Algarve and at Cádiz (Fig. 1). A detailed description of this term is further presented in Section 3.2.5. The along-shore density gradient term can be significant during spring–summer, when river outflow and coastal upwelling may promote strong horizontal density gradients (e.g. Sánchez and Relvas, 2003a,b). However, it is expected to remain generally low during winter, owing to the strong homogenisation and erosion of horizontal gradients, as reported for the California coast (Lentz and Winant, 1986). Unfortunately, a complete hydrographic survey simultaneous to the observations presented here was not undertaken, and so the along-shore density gradient term had to be indirectly estimated. A value of  $\sim 0.4 \text{ kg m}^{-3}$  over 150 km from Cape St. Maria to the Guadalquivir River mouth was calculated from the climatological analysis of a local historic hydrographic database.

The results of the scale analysis are presented in Table 3. The depth-averaged advective term, the

Table 3

Bound values of the terms of the along-shore momentum equation

Term	Bound value ( $10^{-5} \text{ m}^2 \text{ s}^{-2}$ )
$H \frac{\partial \bar{v}}{\partial t}$	4
$H \bar{v} \frac{\partial \bar{v}}{\partial y}$	1
$Hf\bar{u}$	1
$H^2 \frac{g}{\rho_o} \frac{\partial \rho}{\partial y}$	<1
$gH \frac{\partial \eta}{\partial y}$	6
$\frac{\tau_s^w}{\rho_o}$	3
$\frac{\tau_b^b}{\rho_o}$	3
$H\bar{F}$	<1

Coriolis term, as well as the along-shore density gradient term, were, at most, one third of the stress and one fourth of the local acceleration terms, and therefore could be neglected. Caution should be taken if strongly meandering flows (field accelerations), over the middle and outer shelf (across-shelf flows) and/or strong density gradients, such as in frontal zones, are present, since these assumptions may then not be correct. The smallness of the advective term is partly due to the fact that the flow closely follows the isobaths, and it does not suffer from sharp local accelerations (Section 3.2.3). The Coriolis term was assumed zero by necessity, since the proximity of the instruments to the coastal wall set a no-flow condition through the coastal boundary. Additionally, this latter term appeared uncorrelated with other elements of the momentum equation. This observation agrees with previous studies (Lentz and Winant, 1986; Hickey et al., 2003), and shows the lack of dynamical significance of the sub-inertial across-shore velocities, which may probably be related to instrument noise.

After applying the scaling, the Coriolis, advective, along-shore density and Reynolds stress terms may be neglected in the momentum equation. We can rearrange the equation to obtain a linear barotropic expression for the along-shore acceleration:

$$\frac{\partial \bar{v}}{\partial t} = -g \frac{\partial \eta}{\partial y} + \frac{\tau_s^w - \tau_b^b}{H \rho_o}. \quad (5)$$

In this equation, local accelerations are balanced by the gradient of the sea surface (ASLS) and modulated by the difference between the along-shore component of the wind stress and the stress at the bottom of the layer. The relative influence of the stress (surface force) and the ASLS (body force) terms depends on the total depth  $H$  (assumed as constant = 20 m). The scaling of the equation terms (Table 3) indicates that the ASLS was the dominant term in the equation, counteracted by the stress terms to induce the observed motion. As seen in the previous section, low correlations were observed between the flow and local winds. Also outstanding was the fact that local wind velocities were in any case very low, and unlikely to provide the necessary drag to explain the observed accelerations. Hence, an ASLS must exist to account for the residual.

The time series of retained terms in the depth-averaged along-shore momentum Eq. (5) are presented in Fig. 10. We correlated the acceleration and the wind-stress term at the various sites presented in Fig. 1. Flow accelerations in the inner Gulf of Cádiz

(Fig. 10A) were poorly correlated with the along-shore wind stress, measured locally on the south coast (e.g. Faro station  $r = 0.39$ ,  $p < 0.01$ ; Tavira station  $r = 0.42$ ,  $p < 0.01$ ). Conversely, accelerations were well-correlated with the wind stress on the west coast (e.g. Sines station,  $r = 0.89$ ,  $p < 0.01$  or Sagres station  $r = 0.75$ ,  $p < 0.01$ ).

A closer look at the time series gives an understanding of the behaviour of the acceleration, and its association with the along-shore wind stress. For the sake of clarity, the wind stress on the west coast is also presented in Fig. 10B. Maximum eastward accelerations of  $0.16 \text{ m s}^{-1} \text{ d}^{-1}$  were observed between 26 and 27 November, in response to the upwelling-favourable wind event simultaneously observed both on the west and south coasts (Fig. 10A and B).

Similarly, between 29 and 30 November, positive flow accelerations of  $\sim 0.1 \text{ m s}^{-1} \text{ d}^{-1}$  were observed after the presence of northerly winds (on the west coast), although surprisingly, against the local easterlies. Eastward ADCP accelerations occurred well before the full onset of local westerlies occurred at the Cádiz buoy (observe the event marked in Fig. 3). Finally, a smaller pulse of eastward accelerations of  $0.05 \text{ m s}^{-1} \text{ d}^{-1}$  occurred on 5 December, coinciding with a local weakening of the easterlies and enhancement of northerlies on the west coast.

The strongest acceleration event occurred from 30 November to 4 December, with a strong peak of  $0.23 \text{ m s}^{-1} \text{ d}^{-1}$  between 2 and 3 December (Fig. 10). This event reversed the so far eastward flow, resulting in a sharp inversion of the current pattern (see Fig. 8A). This major peak did not seem to be associated with any onset of local easterlies. In fact, one can observe that negative accelerations commenced between 30 November and 2 December, i.e. under the presence of local westerlies (Fig. 3E). The peak in the negative accelerations occurred more than 24 h before any local easterly wind peaks at the Cádiz buoy. Nonetheless, it seemed to occur simultaneously with the strong relaxation of the equatorward component of the wind on the west coast, rather than in association with the strengthening of the local poleward component of the wind.

The inferred ASLS term is presented in Fig. 10D. The plot shows that the sharp current reversal of 1–3 December was associated with the inversion of accelerations forced by the sea-level slope from  $\sim -0.20$  to  $+0.25 \text{ m s}^{-1} \text{ d}^{-1}$ . This value is consistent with the inability of local stresses to counteract the

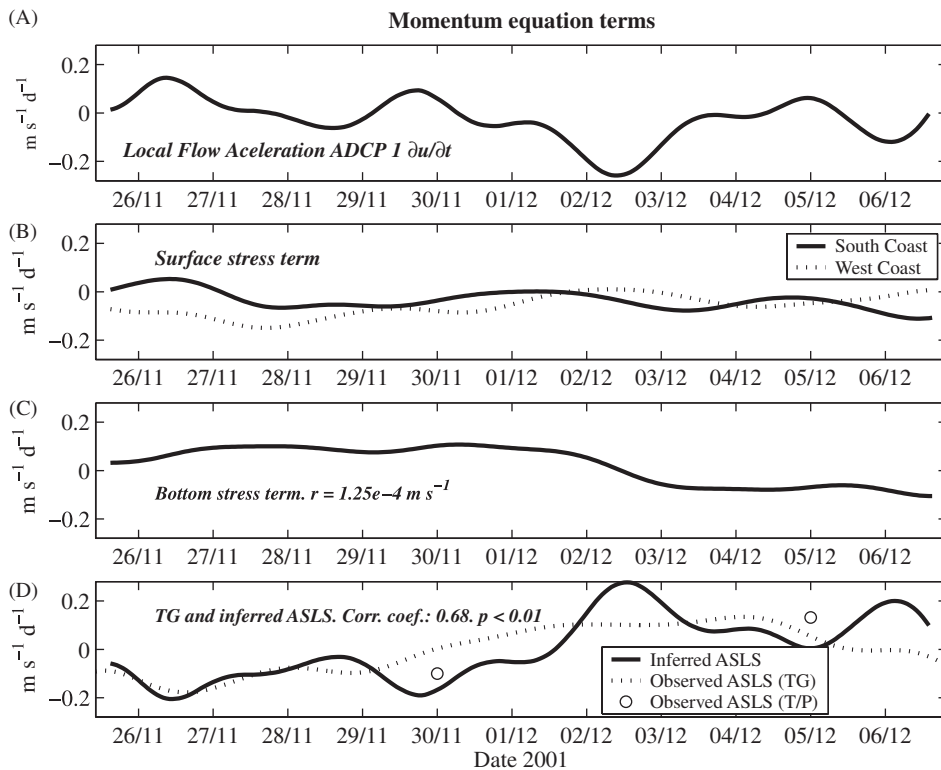


Fig. 10. Terms in the barotropic along-shore momentum Eq. (5). From top to bottom: (A) Local flow acceleration; (B) Surface stress term (solid line). The stress term on the west coast was also plotted for reference (dotted line); (C) Bottom stress term; (D) ASLS  $-g(\partial\eta/\partial y)$  term (TG-observed, dotted line; T/P-observed, open circles). The residual from the difference  $(\tau^s - \tau^b)/H\rho_o - g(\partial v/\partial t)$  is plotted as a bold line. See text for details.

pre-existing ASLS. This makes the ASLS term the main contributor toward the inner-shelf circulation along the eastern Gulf of Cádiz during November–December 2001.

### 3.2.5. Sea-level differences

The linear barotropic momentum equation can be rewritten in terms of the ASLS, as

$$\frac{\partial\eta}{\partial y} = \frac{\tau_s^w - \tau_b^b}{gH\rho_o} - \frac{1}{g} \frac{\partial\bar{v}}{\partial t}. \quad (6)$$

The ASLS inferred using the right-hand side of Eq. (6) has been compared with the ASLS estimated from two local TGs, situated approximately 100 km east and west of the moorings locations, respectively (Fig. 1). Sea-level data were available for the November–December 2001 period (Fig. 11A). The ASLS was estimated as the difference between the sea-level anomalies at the two TGs over a normalised distance of 100 km. ASLS refers to anomalies subtracted from the mean. This ASLS was plotted in Fig. 11B together with the inferred

ASLS from the previous section. The observed ASLS series correlated with the inferred ASLS from the barotropic, linear model. The general trend and the peaks were well simulated by the linear model. The correlation coefficient between both series was 0.69 ( $p < 0.01$ ).

We wanted to estimate this difference by taking another independent measure of the ASLS too. Sea-level anomalies from Topex/Poseidon (T/P) satellite observations were considered. Data were retrieved from the PO.DAAC web gateway (<http://poet.jpl.nasa.gov/>). ASLS was computed by calculating spatial means over two boxes placed either side of Cape St. Vincent, as indicated in Fig. 1. The ASLS was also normalised over a standard distance of 100 km. The T/P data have a maximum temporal resolution of five days, and there were just a few data points for November–December 2001. However, it can be seen that altimetry observations showed a good agreement with both the inferred and TG-observed ASLSs. These values appeared consistent with climatological TG observations

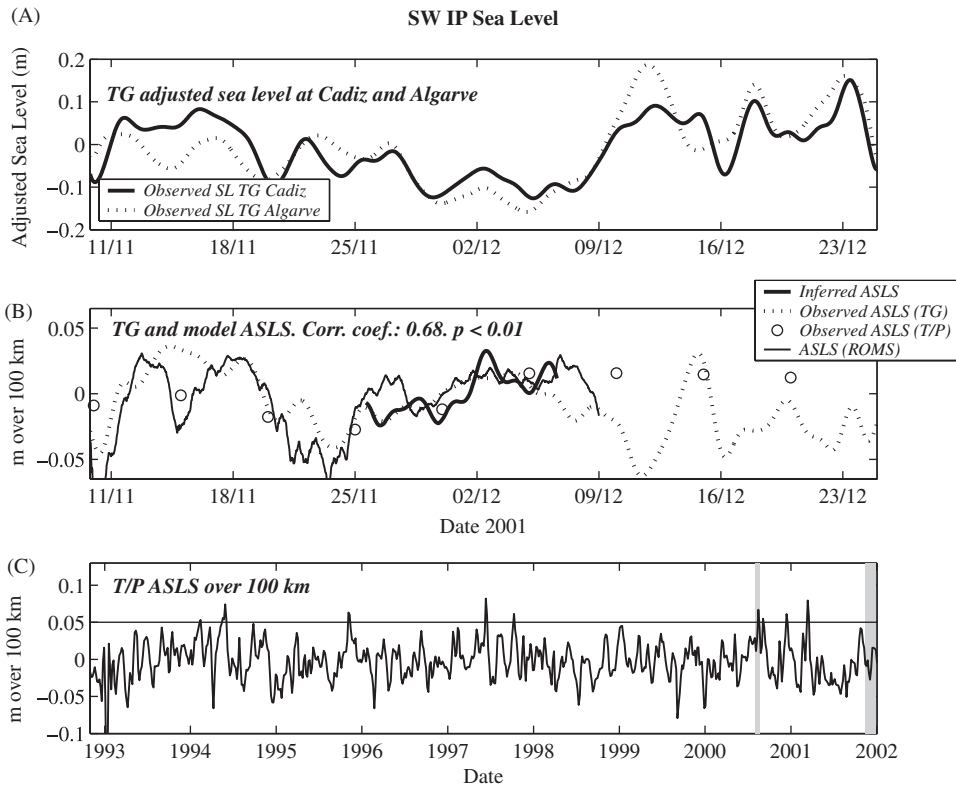


Fig. 11. (A) Inverse-barometer adjusted sea levels at the Cádiz and Algarve tide-gauges for November–December 2001. (B) Along-shore sea-level slope (averaged over 100 km) in November–December 2001 as inferred by the barotropic momentum equation (bold line), the T/P altimeter (open circles) and the difference between the Cádiz and Algarve tide-gauges (dashed line). ASLS modelled by the ROMS simulation is plotted with a thin solid line. (C) ASLS (averaged over 100 km) as inferred by the T/P altimeter. A horizontal line indicates ASLS greater than 5 cm. Grey stripes are referred to in the text.

from Relvas and Barton (2002), who report an ASLS on the order of a few centimeters over 100 km, stronger in summer. These pieces of evidence support the validity of the assumptions taken in the along-shore momentum equation.

### 3.3. Non-linear numerical model for the Gulf of Cádiz

Section 3.2.4 showed that a one-dimensional, linear model was successful at predicting observed accelerations over the northern Gulf of Cádiz. The Regional Ocean Modelling System (ROMS) version 2.1 was used to explore some three-dimensional effects of the combination of complex topography, wind and buoyancy forcing in the Gulf of Cádiz. ROMS features are described in detail in Haidvogel et al. (2003). The model includes a smoothed bottom topography to minimise the gradient pressure error. The domain covers the entire Gulf of Cádiz region, extending between 34.5° and

Table 4  
ROMS simulation parameters

Number of timesteps	8640
Internal (baroclinic) timestep size	500 s
External (barotropic) timestep size	30 s
Surface stretching	5
Bottom stretching	0.4
Thermocline depth	50 m
Open at N, S, W boundaries	Marchesiello et al. (2001)
Horizontal grid resolution	$\Delta x = 4 \text{ km}, \Delta y = 4 \text{ km}$

39.0°N, and 5.5° and 10°W. Further model parameters are given in Table 4. A detailed picture of the model bathymetry in the Gulf of Cádiz is provided in Fig. 13; note the difference between the heavily smoothed model bathymetry and the true bathymetry as in Fig. 6.

The model is started from rest on 20 October 2001 and is run until 8 December 2001. Initialisation is achieved using Gulf of Cádiz winter stratification profiles for 2001 obtained from the World Ocean

Atlas (Hankin et al., 2003). The model is forced using NCEP winds and heat fluxes through a bulk parameterisation. In winter, nearshore regions are frequently occupied by low salinity waters supplied by local rivers (Fig. 7A), hence the need to include fresh water forcing in the model. Fresh water was input at three point sources corresponding to the locations of the three main Gulf of Cádiz rivers: the Guadalquivir River (Alcalá del Río station); the Guadiana River (Pulo do Lobo station); and the Tinto–Odiel River System (12% of the Guadiana outflow, following Cossa et al., 1994). Fig. 7B details the daily outflows from these rivers over the period of the model run.

ROMS SST results are presented in Fig. 12. The figure shows 2-day averages of the SST both before and after the observed current reversal. There is some discrepancy between the temperature values of the model results and the satellite images (c.f. Fig. 6). Nevertheless, the model successfully reproduces the net westward advection of cold water with source on the inner shelf from 26 November to 4 December 2001. Furthermore, along-shore velocity records retrieved from a virtual current meter at the ADCP1 location (Fig. 8A, thin line) show that a current reversal did occur in the model, at about the same time as observed by the ADCPs. Model velocities were in the order of  $\sim 0.04 \text{ m s}^{-1}$ , which is an order of magnitude below our observations. However, we note that, as a result of the smoothing of the bathymetry in the model domain, the depth of the water column at the model ADCP location is 100 m, which is 5 times greater than the true depth of 20 m. A simple correction to the modelled velocity to account for this depth difference may be given by:  $100 \text{ m}/20 \text{ m}$ ; such a correction is not inappropriate, given the volume conservation char-

acteristics of the model, and it produces a model velocity that corresponds to the observed velocities. A model ASLS was retrieved from model TGs situated at approximately the same locations as the observing ones (Fig. 11B, thin line). These data revealed a notably consistent response between the model and the observations.

In order to isolate the effects of the wind stress from the buoyancy forcing a secondary set of simulations was conducted without the river input (not shown). These model results revealed qualitatively similar results as the with-river results, although the absolute values of the along-shore momentum were offset. As such, a current shift occurred at about the same time as observed in the data (see Section 3.2.3), independently of the presence of the buoyant water. This was not a surprise since the river discharge values remained low during the simulation period (Fig. 7B). Hence, the model current shift is not attributed to the presence of a buoyant river plume.

The temporal coincidence in the response of the model with the observations suggests that the development of the counter-current at the beginning of December 2001 was a response to a combination of wind stress and topography. In this respect, it was noted that the NCEP winds (used to force the model) showed a strong degree of similarity with the wind fields shown in Fig. 4, satisfactorily reproducing the coastally induced contortions of the wind flow around Cape St. Vincent.

#### 4. Discussion

As Lentz and Winant (1986) observed, studies that show correlation between current structure, SST signatures and along-shore winds, have

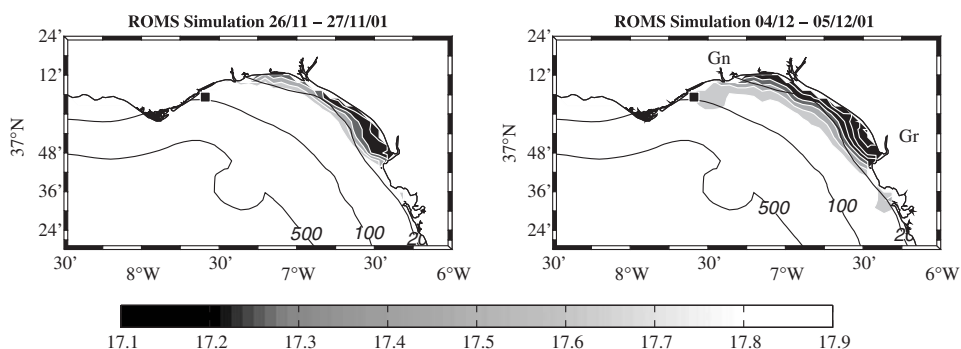


Fig. 12. Model SST fields. (A) 26–27 November 2001, (B) 4–5 December 2001. Labels Gn and Gr stand for Guadiana and Guadalquivir rivers, respectively. Colourbar units are degrees Celsius. A black square denotes the ADCP1 location. Smoothed 20, 100 and 500 m bathymetric contours are also plotted. Note the difference from the true bathymetric contours as in Fig. 6.

typically been made in regions characterised by strong winds. In contrast, when the local wind stress is weak relative to other forcing terms in the equation of motion, this local correlation is degraded by necessity. The perception of the northern Gulf of Cádiz as a region sheltered from the main offshore winds aids understanding of the reasons for the lack of correlation between the SST signature and local winds, as reported in recent studies (Peliz et al., 2004). These facts make the northern margin of the Gulf of Cádiz a good candidate for a study of a wind-sheltered region.

Fig. 13 shows four snapshots of the development of the inner-shelf counter-current in the first half of August 2000. Mean (subinertial) wind vectors over a 48-h period prior to the image acquisition are also plotted, together with a sequence of cloud-free SST

daily composite images at 4-day intervals. From 4 to 8 August the vigorous upwelling-favourable wind ( $>10 \text{ m s}^{-1}$ ), relaxed north of  $37^\circ\text{N}$  and shifted to easterly, in the Gulf of Cádiz (Fig. 13A and B). This permitted the development of an inshore (warm) flow that reached and turned around Cape St. Vincent on 8 August. After this date the flow continued poleward, in spite of the return of the equatorward, upwelling-favourable winds. This event resulted in the break-up of the upwelling pattern west of Cape St. Vincent. As for the results of the ADCP survey of November–December 2001 presented in the previous section, lack of correlation between local winds and SST was shown.

The energetic event presented in Fig. 13 shows a counterflow that breaks through the equatorward cold flow, separating the eastern and southern cold

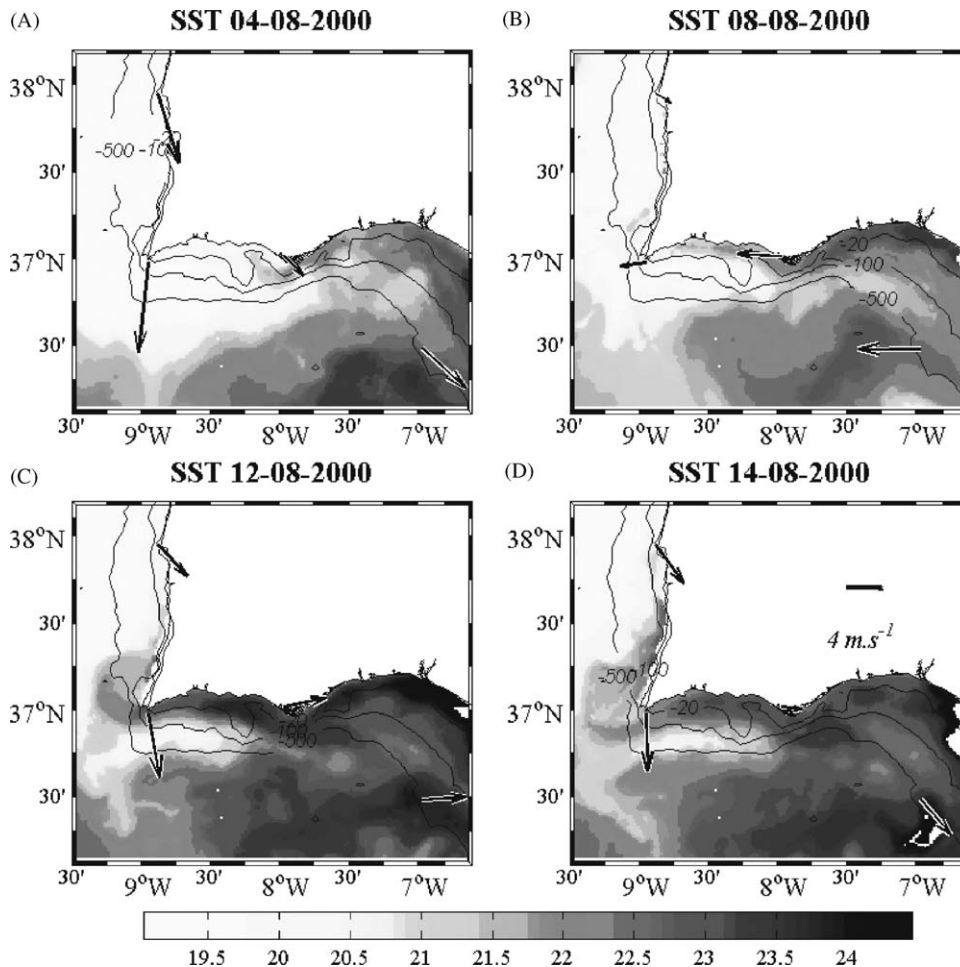


Fig. 13. Sequence of AVHRR SST for the first half of August 2000. Wind vectors at the Sines, Sagres, Faro, and the Cádiz buoy anemometer stations are also presented, and correspond to averages over the 24 h prior to the image capture. Reference vector is  $4 \text{ m s}^{-1}$ . Colourbar units are degrees Celsius. (A) 4 August; (B) 8 August; (C) 12 August; (D) 14 August.

features. This latter situation is a rare feature seldom observed in the SST imagery. From 1982 to 1995, with the help of daily SST images, Relvas and Barton (2002) reported just seven such occurrences. We looked up the updated SST database with weekly SST images from 1994 to 2002, obtained from the German Remote Sensing Service (<http://isis.dlr.de/>). Breakthrough signals in the weekly composites indicated events persisting for at least one week. For this period, breakthrough episodes could be observed 3 times, namely during the weeks starting on 7 August 2000, 11 September 2000 and 29 October 2001.

In Fig. 11C the 1992–2002 ASLS as observed by the T/P altimeter is presented. It also has been referenced over a standard 100 km distance. A straight line marks the 5 cm ASLS threshold. Shaded stripes denote the August 2000 event from Fig. 13 and the November–December 2001 survey. Over 1992–2002, the ASLS rarely exceeded 5 cm above the mean. It can be seen that in August 2000 the ASLS exhibited one of the largest positive peaks, featuring values in excess of 7 cm. Ignoring the stress terms, and considering just the ASLS and acceleration terms in the equation of motion (e.g. Eq. (6)), we can estimate crudely the acceleration forced by the ASLS alone to be  $\sim 0.5 \text{ m s}^{-2}$ . This value approximates the values obtained if we take the thermal contrast of SST images as a tracer of the flow from the daily sequence of SST images (Fig. 13). Hence, in this case and as was observed from the November–December 2001 observations, the existence of an ASLS capable of forcing inner-shelf poleward motion seems reasonable.

Results presented here verified the existence of an ASLS, responsible for the inshore flow under the presence of weak local winds. In Section 3.2.4 it was observed that during November–December 2001, local winds over the northern Gulf of Cádiz as measured at three anemometer wind stations, were relatively weak when compared with other forcing terms. The ASLS emerged as the main contributor to the dynamical balance in Eq. (6). The inability of local wind stress to counteract the existing ASLS permitted a sharp current reversal that brought about, among other consequences, westward advection of colder waters that prompted a dramatic temperature drop over a single local inertial period ( $\sim 19.9 \text{ h}$ ).

The question of the origin of this ASLS is unclear. A number of mechanisms can be proposed as responsible for its generation. First, influence of

the mixing with the shallow Mediterranean Outflow Water (MOW) in the northern Gulf of Cádiz (Mauritzen et al., 2001) provides a scenario that may help to explain the existence of a local sea-level gradient. More general mechanisms applicable to other similar zones include the effects related to buoyant plumes and the wind stress and its curl.

Considering the influence of the MOW, Mauritzen et al. (2001) concluded that the inshore circulation above the core of Mediterranean water is westward. They argued that the effects of local mixing with the MOW would favour the formation of an inner-shelf, topographically steered, westward surface density current. The effects of buoyant plumes on the upper-layer circulation in the northern Gulf of Cádiz were considered by Peliz et al. (2004). These authors observed that low-salinity water with source in the fluvial runoff can at times interact with the topography and the offshore eddy field, resulting in dramatic westward-extending river plumes. Model results presented in Section 3.3 were able to reproduce broadly the characteristics of the current shift event of November–December 2001 without explicitly introducing the MOW or the river input (Fig. 12). These results suggest that the problem should be centred on interaction between the wind and topographic forcing. More specifically: is the onshore Ekman transport able to promote an ASLS that could trigger the development of a coastal counter-current, or is the ASLS formed by dissimilar wind-stress forcing either side of Cape St. Vincent? Numerical model analyses carried out for similar regions have revealed that heterogeneities in the wind field may generate along-shore gradients of the oceanic curl of the wind stress, that can be exclusively invoked as a major mechanism responsible for the generation of a local ASLS (Oey et al., 2001).

In this sense, the change of orientation of the coast at Cape St. Vincent, and the proximity of the coastal margin to the nearby mountain chains (Fig. 1), provide a disrupting effect on the synoptic wind field, breaking the spatial coherence of coastal and ocean winds around the SW IP and hence generating the local forcing. From Fig. 2 the spatial vector correlation length scales indicate that this spatial heterogeneity in the wind field appears smaller than its purely atmospheric scales of variation (Sánchez et al., 2005). This heterogeneity may be associated with the presence of Cape St. Vincent. As an example, mean winds over the northern Gulf of Cádiz shelf are much weaker than

those in exposed areas (cf. Fig. 1) from which the perception of a dual wind pattern either side of the Cape emerges. These results provide evidence for the apparent orographically induced shadowing and deformation of the large-scale ocean wind field over the Cape St. Vincent region.

The spatial heterogeneity of the coastal winds has an influence on the coastal circulation over sheltered regions in the lee of Cape St. Vincent. Sánchez and Relvas (2003a,b) considered the comprehensive ocean atmosphere data set (COADS) monthly mean winds. These authors observed local divergences in the Ekman layer from May to September. Local positive maximum wind-stress curl was associated with Cape Finisterre and Cape St. Vincent, which introduced the major coastline irregularities in the western IP region. The climatological winds featured vertical velocities of  $0.2 \text{ m d}^{-1}$  close to these Capes. Heterogeneity of ocean winds near Cape Finisterre has been observed in the QuikSCAT analysis of Torres et al. (2003). Owing to the finer spatial resolution ( $0.25^\circ$ ) than those of COADS, pumping velocities in excess of  $6 \text{ m d}^{-1}$  were inferred. Münchow (2000) showed strong wind-stress curl in the lee of the prominent Point Conception (California), a coastal configuration much akin to Cape St. Vincent. This author used aircraft-based winds with great spatio-temporal resolution, permitting the observation of strong cyclonic circulation, that may result in upward Ekman pumping velocities greater than  $20 \text{ m d}^{-1}$ .

To further understand the wind effect on sea level, we correlated the sea level at the TGs in the Gulf of Cádiz and the along-shore component of the wind stress at several locations along the western IP and North Africa for the period 1 November–1 December 2001 (Fig. 14A, see inset for locations). The wind sources were the southwestern IP anemometer wind stations (plotted as solid dots in the inset of Fig. 14) and NCEP Reanalysis 10-m winds (plotted as empty circles in the inset of Fig. 14). Mean NCEP wind vectors for this period are also plotted. The locations of the TGs are indicated by asterisks. Following Hickey et al. (2003), we retained just the long-period component by considering either wind or sea-level fluctuations longer than 10 days. There was a general trend showing higher correlations between the TG sea levels and the along-shore winds, following the  $10^\circ \text{W}$  line from north to south. This can be interpreted as a consequence of the large-scale nature of the wind outside the Gulf of Cádiz, rather than the result of

an oceanic process. Considerably weaker correlations were observed for comparisons between the TG and local winds in the Gulf of Cádiz, a correlation low being observed between  $39^\circ \text{N}$  and  $32^\circ \text{N}$ , where values were always  $< 0.8$ . These results clearly suggest that winds in the Gulf of Cádiz are unable to explain the local sea-level response. Rather, this response is better correlated with the remote winds.

In Fig. 14B we present the meridional correlations between the ASLS and the zonal shear of the along-shore wind stress, at several locations along  $12.5^\circ \text{W}$ – $10^\circ \text{W}$  in the western IP. Within confidence limits, sea-level gradients in the Gulf of Cádiz showed good correlations ( $> 0.7$ ) with the zonal shear of the along-shore wind stress close to the coast north of  $30^\circ \text{W}$ . These may be attributed to the heterogeneity of the large-scale winds when approaching the coast, as was observed in Section 3.1. In the vicinity of the Gulf of Cádiz region, this heterogeneity may be implicated in the generation of dissimilar upwelling-/downwelling-favourable wind patterns either side of Cape St. Vincent (cf. Fig. 4).

The effect of the large-scale wind heterogeneity upon the ASLS is illustrated in Figs. 3 and 11A. Upwelling-favourable winds before 28 November contributed to the general sea-level drop observed by both TGs. From 29 November the sea level on the west coast remained relatively low, as a result of the re-intensification of local upwelling-favourable winds. In contrast, the sea level over the inner Gulf of Cádiz increased sharply, probably after the sustained onshore transport of the local easterlies during 28–30 November. This conjunction contributed to the construction of a local along-shore pressure gradient, that if not balanced by the local wind stress may be held responsible for the poleward propagation, as has been proposed by Relvas and Barton (2002).

These processes may trigger the generation of a coastally trapped wave (CTW). CTWs propagate along the continental margins of many of the world's oceans with the coast on the right in the northern hemisphere with periods ranging from a few days to weeks. The study of generation and evolution of a CTW was outside the scope of this paper. It is argued, instead, that heterogeneities in the wind field can be responsible for the initiation of a poleward circulation in a similar manner to the propagation of CTW reported in similar areas, where they have been seen to account for a major

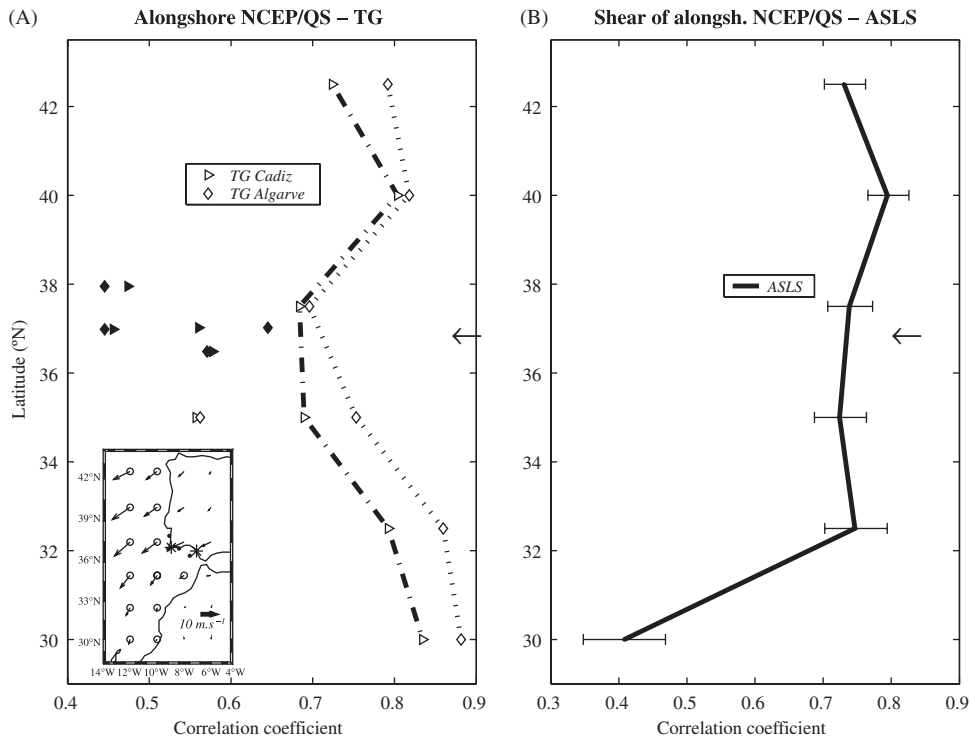


Fig. 14. (A) Maximum correlation between the along-shore component of the wind stress at selected latitudes and observed sea level at Cádiz and Algarve tide-gauges (TG) for the period 1 November–31 December 2001. The time lag ranges 7–12 days for all cases. The 95% confidence level is below 0.4 in all cases. The correlation values ( $x$ -axis) are latitudinally sorted from north to south ( $y$ -axis). Empty symbols refer to correlations between the NCEP winds and each of the TGs. Solid symbols refer to correlations between the anemometer wind stations (Sines, Sagres, Faro and Cádiz) and each of the TGs. For reference, the correlations along the  $10^{\circ}\text{W}$  line are joined with a line for each TG. The inset indicates the location details: AW stations are plotted as solid dots; TG locations are plotted as asterisks; NCEP 10-m reanalysis winds are plotted as empty circles; mean NCEP wind vectors for November–December 2001 are also plotted. See Fig. 1 for a detailed picture. (B) Maximum correlation between the zonal shear of the along-shore component of the NCEP wind stress at selected latitudes and observed along-shore sea-level slope between the Cádiz and Algarve TGs for the period 1 November–31 December 2001. Confidence bounds are also plotted. A black arrow approximately indicates the latitude of the TG stations.

part of the nearshore low-frequency variability (Hickey et al., 2003; Pringle and Riser, 2003). This nearshore transport might have broad implications for both the biological and pollution dynamics in this region.

## 5. Summary and conclusions

- The alternating nature of the coastal flow along the southwestern IP in the Gulf of Cádiz has been shown, using satellite images and in situ temperature and velocity data, for the period November–December 2001. Of particular interest was a sharp current inversion, that occurred over 2 days and was uncorrelated with the local wind stress.
- During deployments conducted in November–December 2001, the Coriolis, advective and

along-shore density terms could be neglected from the along-shore barotropic momentum equation. The resulting balance showed that the inversion of the flow had to be associated with a sharp change in ASLS of  $\sim 5$  cm over 100 km.

- The analysis of anemometer wind station data along the southwestern IP, collected over a 777-day period showed that the general wind pattern along the eastern Atlantic suffers from strong shadowing in the Cape St. Vincent region, the wind stations being well-correlated along each perpendicular coast, but uncorrelated with the stations on the opposing coasts. The introduction of a sharp spatial heterogeneity in the wind field by the Cape and the nearby coastal mountain chains may generate along-shore gradients of the oceanic wind stress, which in turn contribute to the circulation patterns in the Gulf of Cádiz. This

had an anomalously strong effect during November–December 2001.

- Results from a non-linear three-dimensional model run for October–December 2001 considering wind stress, topography and weak fluvial input as the forcing terms, rendered flow patterns temporally coincident with the observations. These results suggest that the problem should be centred on the interaction between the wind and topographic forcing.
- Sea-level variability is mostly explained by relaxation of equatorward winds on the windward side of Cape St. Vincent, rather than by local wind forcing. This was attributed to the heterogeneity of the large-scale winds when approaching the coast in the Gulf of Cádiz region. The mechanism is associated with the dissimilar generation of upwelling-/downwelling-favourable wind patterns either side of Cape St. Vincent.
- Regional features, such as the large-scale wind-stress field, are important in fully representing detailed aspects of the circulation in the coastal zone, and have to be properly taken into account to model the circulation in the Gulf of Cádiz. This highlights the importance of coupling of the local model with a regional model.

### Acknowledgements

The present work benefited from the CIMA-UAlg, ATOMS (FCT contract PDCTM/P/MAR/15296/1999) and SIRIA (Situação de referência da Região costeira algarvia Influenciável pelo funcionamento da barragem de Alqueva) projects. Evan Mason is funded by the project PELAGICOS (FCT PLE/13/00). Tide gauge levels were obtained from the Instituto Hidrográfico da Marinha (Portugal) and Puertos del Estado (Spain). The authors would like to express their gratitude to Puertos del Estado and the RAYO project for making available the Cádiz buoy data, specially to B. Morón and E.A. Fanjul. QuikSCAT data were obtained from the NASA Physical Oceanography Distributed Active Archive Center at the Jet Propulsion Laboratory/California Institute of Technology. Other wind data were obtained from the Instituto de Meteorologia (Portugal), for which we are grateful. We would like also to acknowledge the German Remote Sensing Service (Deutsches Zentrum für Luft-und Raumfahrt, DLR) for the AVHRR satellite imagery. We thank also the NOAA-CIRES Climate Diagnostics

Center, Boulder, Colorado, USA, (<http://www.cdc.noaa.gov/>) for the distribution of NCEP data. QSCAT/NCEP Blended Ocean Winds from Colorado Research Associates (version 4.0) were provided by the Data Support Section of the Scientific Computing Division at the National Center for Atmospheric Research, from their web site (<http://dss.ucar.edu/datasets/ds744.4/>). We thank CHG (Spanish Ministry of Environment) and INAG (Portuguese Ministry of Environment) for the river discharge data. Finally, we are indebted to the crew of the R/V Andrómeda, and the technical personnel of the IH.

### References

- Breaker, L.C., Gemmill, W.H., Crosby, D.S., 1994. The application of a technique for vector correlation to problems in meteorology and oceanography. *Journal of Applied Meteorology* 33 (11), 1354–1365.
- Chin, T.M., Milliff, R.F., Large, W.G., 1998. Basin-scale, high-wavenumber sea surface wind fields from a multiresolution analysis of scatterometer data. *Journal of Atmospheric and Oceanic Technology* 15, 741–763.
- Cossa, D., Elbaz-Poulichet, F., Nieto, J.M., 1994. Mercury in the Tinto–Odiel estuarine system (Gulf of Cadiz, Spain): sources and dispersion. *Aquatic Geochemistry* 7, 1–12.
- Crosby, D.S., Breaker, L.C., Gemmill, W.H., 1993. A proposed definition for vector correlation in geophysics: theory and application. *Journal of Atmospheric and Oceanic Technology* 10, 355–367.
- Fiúza, A., 1983. Upwelling patterns off Portugal. In: Suess, E., Thiede, J. (Eds.), *Nato Conference Series IV Marine Science*, vol. 10a, Coastal Upwelling: Its Sediment Record, pp. 85–98.
- Folkard, A.M., Davies, P.A., Fiúza, A., Ambar, I., 1997. Remotely sensed sea surface thermal patterns in the Gulf of Cádiz and the Strait of Gibraltar: variability, correlations, and relationships with the surface wind field. *Journal of Geophysical Research* 102 (C3), 5669–5683.
- Haidvogel, D.B., Arango, H.G., Hedstrom, K., Beckmann, A., Malanotte-Rizzoli, P., Shchepetkin, A.F., 2003. Model evaluation experiments in the North Atlantic Basin: simulations in nonlinear terrain-following coordinates. *Dynamics of Atmospheres and Oceans* 32, 239–281.
- Hankin, S., Callahan, J., Sirott, J. 2003. The live access server and DODS: web visualization and data fusion for distributed holding. Available at: (<http://ferret.pmel.noaa.gov/Ferret/LAS/LASoverview.html>).
- Hickey, B.M., Dobbins, E.L., Allen, S.E., 2003. Local and remote forcing of currents and temperature in the central Southern California Bight. *Journal of Geophysical Research* 108 (C3), 10.1029/2000JC000313.
- Kundu, P.K., 1976. Ekman Veering Observed near the Ocean Bottom. *Journal of Physical Oceanography* 6, 238–242.
- Large, W., Pond, S., 1981. Open ocean momentum flux measurements in moderate to strong winds. *Journal of Physical Oceanography* 11, 324–336.

- Lentz, S.J., Winant, C., 1986. Subinertial currents on the Southern California Shelf. *Journal of Physical Oceanography* 16, 1737–1750.
- Lobo, F.J., Sánchez, R., González, R., Dias, J.M.A., Hernández-Molina, F.J., Fernández-Salas, L.M., Díaz del Río, V., Mendes, I., 2004. Contrasting styles of the Holocene high-stand sedimentation and sediment dispersal systems in the northern shelf of the Gulf of Cádiz. *Continental Shelf Research* 24 (4–5), 461–482.
- Marchesiello, P., McWilliams, J.C., Shchepetkin, A.F., 2001. Open boundary conditions for long-term integration of regional oceanic models. *Ocean Modeling* 3, 1–20.
- Mauritzen, C., Morel, Y., Paillet, J., 2001. On the influence of Mediterranean Water on the Central Waters of the North Atlantic Ocean. *Deep-Sea Research I* 48, 347–381.
- Münchow, A., 2000. Wind-stress curl forcing of the coastal ocean near point conception, California. *Journal of Physical Oceanography* 30, 1265–1280.
- Oey, L.-Y., Wang, D.-P., Hayward, T., Winant, C., Hendershott, M., 2001. Upwelling and cyclonic regimes of the near-surface circulation in the Santa Barbara channel. *Journal of Geophysical Research* 106 (C5), 9213–9222.
- Peliz, A., Santos, A.M., Oliveira, P.B., Dubert, J.D., 2004. Extreme cross-shelf transport induced by eddy interactions southwest of Iberia in winter 2001. *Geophysical Research Letters* 31, L08301.
- Pringle, J.M., Riser, K., 2003. Remotely forced nearshore upwelling in Southern California. *Journal of Geophysical Research* 108 (C4), 3131.
- Relvas, P., Barton, E.D., 2002. Mesoscale patterns in the Cape São Vicente (Iberian Peninsula) upwelling region. *Journal of Geophysical Research* 107 (C10), 3164.
- Relvas, P., Barton, E.D., 2005. A separated jet and coastal counterflow during upwelling relaxation off Cape São Vicente (Iberian Peninsula). *Continental Shelf Research* 25, 29–49.
- Sánchez, R., Relvas, P., 2003a. Spring–summer climatological circulation in the upper layer in the region of Cape St. Vincent, SW Portugal. *ICES Journal of Marine Science*, doi:10.1016/S1054-3139(03)00137-1.
- Sánchez, R., Relvas, P., 2003b. Poleward counter-currents during the upwelling season along SW Portugal. EGS-AGU-EUG Joint Assembly (Nice, France, 6–11 April 2003). *Geophysical Research Abstracts*, vol. 5, EAE03-A-12313.
- Sánchez, R., Relvas, P., 2005. Coupled wind and sea surface temperature patterns along SW Iberian Peninsula. *Journal of Marine Systems*, submitted for publication.
- Sánchez, R., Relvas, P., Pires, H.O., 2005. Comparisons of ocean scatterometer and anemometer winds off SW Iberian Peninsula. *Continental Shelf Research*, submitted for publication.
- Torres, R., Barton, E.D., Miller, P., Fanjul, E., 2003. Spatial patterns of wind and sea surface temperature in the Galician upwelling region. *Journal of Geophysical Research* 108 (C4), 3130.